Intracellular Encoding of Spatiotemporal Guidance Cues in a Self-Organizing Signaling System for Chemotaxis in *Dictyostelium* Cells

Tatsuo Shibata,[†‡§*] Masatoshi Nishikawa,[†§] Satomi Matsuoka,[§¶] and Masahiro Ueda[§¶||]

[†]Laboratories for Physical Biology, RIKEN Center for Developmental Biology, Kobe, Japan; [‡]PRESTO, Japan Science and Technology Agency (JST), Saitama, Japan; [§]Japan Science and Technology Agency (JST), CREST, Osaka, Japan; [¶]Laboratory for Cell Signaling Dynamics, RIKEN Quantitative Biology Center, Osaka, Japan; and [||]Laboratory of Single Molecule Biology, Graduate School of Science, Osaka University, Osaka, Japan

ABSTRACT Even in the absence of guidance cues, chemotactic cells are often spontaneously motile, which should accompany a spontaneous symmetry breaking inside the cells. A shallow chemoattractant gradient can induce these cells to move directionally without much change in cell morphology. As the gradient becomes steeper, the accuracy of chemotaxis increases. It is not clear how the steepness is expressed or encoded internally in the signaling network, which in turn coordinately activates the motile apparatus for chemotaxis. In *Dictyostelium* cells, self-organizing polarization activities in the signaling network have been reported. In this paper, we conducted a theoretical study of the response of this self-organizing system to guidance cues. Our analyses indicate that self-organizing systems respond sharply to a shallow external gradient by increasing the precision of polarity direction and modulating the frequency of self-polarization. We also show how the precision increase and frequency modulation are achieved. Our results indicate that self-organizing activity, independent of external cues, is the basis for the sensitive and robust response to shallow gradients. Finally, we show that the system can sense the direction of space-time waves of a stimulus, for which *Dictyostelium* cells exhibit chemotaxis in the developmental process.

INTRODUCTION

The ability of cells to sense an external chemical gradient is essential to cellular functions such as chemotaxis and other diverse processes (1). Eukaryotic cells such as leukocytes, neurons, and amoebae detect differentials in the concentration of chemicals along their periphery, without rapid motile translocation. A concentration differential of a few percent across a cell body of a few tens of micrometers can be sufficient to induce directional migration. In addition, the gradient information must be maintained in the presence of noise in the signaling network and amplified sufficiently for downstream processes to produce directional migration (2,3). What type of gradient sensing mechanism can afford such astonishing sensitivity in noisy cellular systems?

In *Dictyostelium discoideum*, several signaling pathways have been identified to mediate chemotaxis in parallel (4–6). Among them, the phosphatidylinositol (PtdIns) lipids reaction is the key signaling event responsible for chemotaxis in a shallow chemoattractant gradient (7). The PtdIns signaling pathway also works for chemotaxis in other eukaryotic cells (8). Along a chemoattractant gradient, phosphoinositide-3-kinase (PI3K) catalyzes the production of PtdIns(3,4,5)P3 from PtdIns(4,5)P2 at the membrane region facing the higher chemoattractant concentration, whereas the phosphatase and tensin homolog (PTEN) catalyzes the reverse reaction in the membrane region facing the lower concentration. As a result, accumulation of PtdIns(3,4,5)P3 induces actin polymerization to form a pseudopod in the region of higher chemoattractant, leading to chemotaxis. However, accumulation of PtdIns(3,4,5)P3 can be induced even in the absence of a gradient. *Dictyostelium* cells exhibit random cell migration using the same motility apparatus (9–12). We hypothesized that some type of intracellular signaling must be spontaneously produced at random positions to polarize and activate the motility apparatus.

Spontaneous activity of chemotaxis systems in the absence of a chemical gradient have been reported previously, including cell motility (13,14), actin waves (15–17), and formation of PtdIns(3,4,5)P3–localized domains (18–22). We reported recently that the PtdIns lipids system is responsible for generating spontaneous signals that promote random cell migration (21). In the absence of an external gradient, the PtdIns lipids system can self-organize to produce a domain of high PtdIns(3,4,5)P3 concentration on the membrane (21,23), as shown in Fig. 1 *A* and *B*. The domain exhibits a variety of spatiotemporal dynamics, such as persistent domain formation, that lasts for more than 30 min (Fig. 1 *A*, left), and transient domain formation lasts 10 s to 1 min (Fig. 1 *B*, left). We have proposed a model to explain the mechanism of these self-organization activity, which was developed based on spatiotemporal statistical analysis of fluorescence image

Submitted April 13, 2013, and accepted for publication September 23, 2013.

*Correspondence: tatsuoshibata@cdb.riken.jp

M. Nishikawa's present address is Max Planck Institute of Molecular Cell Biology and Genetics, Dresden, Germany.

Editor: Edda Klipp.

0006-3495/13/11/2199/11 $2.00

http://dx.doi.org/10.1016/j.bpj.2013.09.024

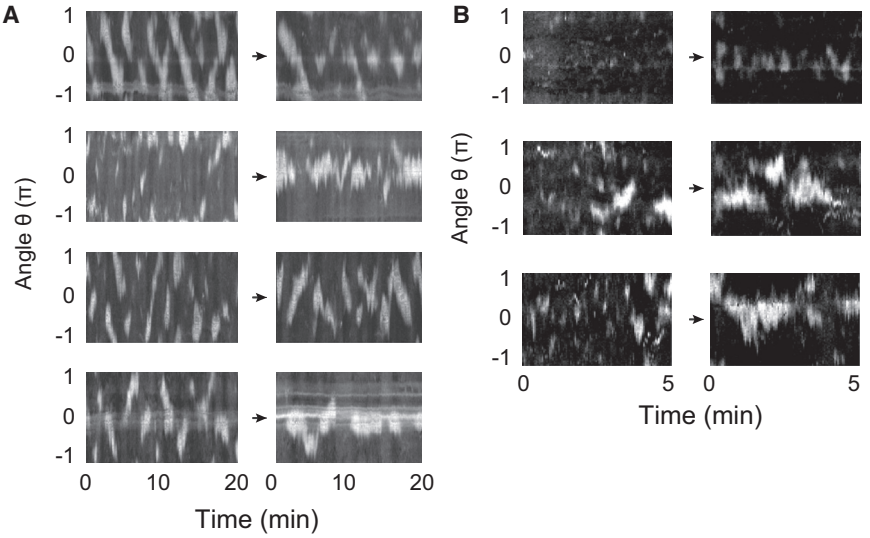

FIGURE 1 Self-organization of the PtdIns signaling reaction. (*A*,*B*) The intensities of PH–GFP along the membrane are plotted with the angle θ and time t, before (*left*) and after (*right*) applying cAMP gradients. (*A*) Persistent formation of PH-GFP–enriched domains. The cells were treated with 4 mM caffeine. (*B*) Transient formation of PH-GFP–enriched domains.

data of single cells (23). This model exhibits a variety of behaviors (Fig. 2 *B–D*). In particular, the model reproduces two kinds of behaviors that were observed experimentally (compare Fig. 1 *A* and *B* and Fig. 2 *C* and *D* in the absence of gradient): first, PtdIns(3,4,5)P3–enriched domains form transiently at random positions (Fig. 2 *D*); and second, the domains form persistently and travel on the membrane (Fig. 2 *C*). These behaviors are related to excitable and oscillatory properties of the local signaling reaction (23). Therefore, depending on the parameter values, this model shows the three types of behaviors in the absence of a gradient: 1) quiescent state (Fig. 2 *B* for the first 30 min); 2) transient domain formation (Fig. 2 *D* for the first 30 min); and 3) persistent domain formation (Fig. 2 *C* for the first 30 min). Since PtdIns(3,4,5)P3 guides the pseudopod position, self-organizing domains can function as preformed internal guidance or an intrinsic compass, independent of external cues. How does this self-organized compass respond to external gradients? In particular, can such self-organized activity contribute to high sensitivity to a shallow gradient? In this paper, we conducted a theoretical study

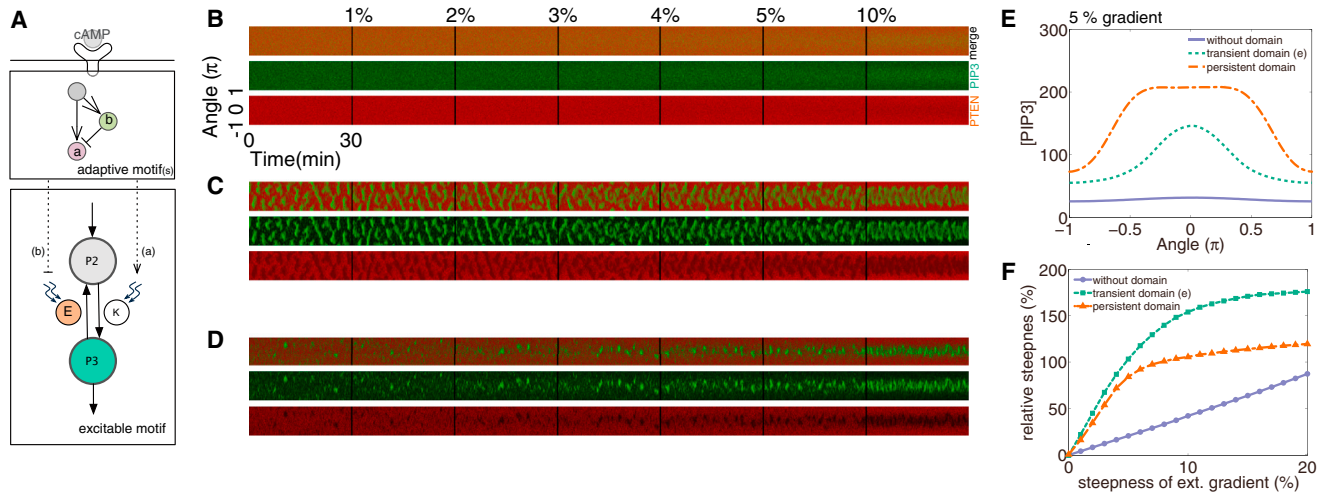

FIGURE 2 Responses of the self-organized PdtIns lipid reaction to external gradient. (*A*) Model of the chemotaxis signaling system consisting of excitable motif and adaptive motif. P2, P3, E, and K denote PtdIns(4,5)P2, PtdIns(3,4,5)P3, PTEN, and PI3K, respectively. The dotted arrows indicate the stimulus from upstream signaling reactions. (*B–D*) Kymographs of [PIP3] (*green*) and [PTEN] (*red*) responses to external gradients (*B*) without spontaneous domain formation, (*C*) with persistent domain formation, and (*D*) with spontaneous transient domain formation. The external gradient directed to the angle of zero increases every 30 min from 0% to 10%. $V_{PI3K} = 320$ and $\lambda_2 = 0.005$ s^{-1} (*B*), 600 and 0.005 (*C*), and 560 and 0.01 (*D*). (*B–D*) $k = 45$ molecules μm^{-2}s^{-1}, $V_E = 15$s^{-1}, $K_1 = 50$ molecules μm^{-2}, $K_2 = 3500$ molecules μm^{-2}, $\lambda_3 = 0.2$ s^{-1}, $V_{ass} = 1300$ molecules μm^{-2}μM^{-1}s^{-1}, $K_4 = 120$ molecules μm^{-2}, $K_5 = 3000$ molecules μm^{-2}, $D_P = 0.2$ μm^2 s^{-1}, $\lambda_E = 1$ s^{-1}, $D_E = 0.15$ μm^2 s^{-1} $E_t = 0.1$ μM. (*E*) Temporal average of the distribution of [PIP3], with a 5% gradient applied between front and back, for cases without spontaneous domain formation (*blue*), with spontaneous transient domain formation (*green*), and with persistent domain formation (*red*). (*F*) Relative steepness in [PIP3] plotted against the external steepness.

of the response of the self-organizing PtdIns lipids signaling system to external gradients.

Numerous mathematical models have been proposed to elucidate the mechanisms of gradient sensing (24). In particular, mechanisms involving self-organizing behaviors have been proposed on the basis of nonlinear mechanisms of wave generation (25), bistability (26), phase separation (27), and excitability (23,28,29). In this paper, based on the model proposed previously, we show that the self-organizing system can exhibit sharp responses to shallow gradients of external chemoattractant. The system accomplishes this by increasing the positional precision of the localized signaling domain and modulating the frequency at which these domains are formed. We also show how the precision and frequency can be modulated. Thus, we demonstrate that the self-organizing activity in the absence of cues is a basis for the high degree of responsiveness to external gradients. Finally, we show that the system can also sense the direction of space-time waves from a stimulus, which is a critical ability in *Dictyostelium* development. The essential aspect of our result is not restricted to the gradient sensing of *Dictyostelium* but can be also applicable to eukaryotic chemotaxis of mammalian cells and gradient sensing in diverse systems.

MATERIALS AND METHODS

Cell preparation

Cell construction and growth conditions were as described previously (21). Before fluorescence imaging, cells expressing $PH_{Akt/PKB}$-EGFP were starved by suspension in development buffer (DB: 5 mM Na phosphate buffer, 2 mM $MgSO_4$, 0.2 mM $CaCl_2$, pH 6.3) for 1 h, and pulsed with 10 nM cAMP at 6-min intervals for up to 3.5 h, leading to the polarized cell shape that indicates chemotactic competency. Cells shown in Fig. 1 *A* and *B* were then settled in DB in the presence of 4 mM caffeine and 5 μM latrunculin A (L5163, Sigma; Fig. 1 *A*), and in the presence of 5 μM latrunculin A (Fig. 1 *B*), and incubated for 20 min. For caffeine-free cells (Fig. 1 *B*), cell density was kept under 5×10^3 cells/mL to eliminate cell-to-cell interactions via secreted cAMP. In Fig. 1 *A*, for the first 20 min, cells were observed without cAMP stimulation. For the last 20 min, a cAMP gradient was applied to the same cells by micropipette filled with 1 μM cAMP (see Microscopy). In Fig. 1 *B*, for the first 5 min, cells were observed without cAMP stimulation. For the last 5 min, a cAMP gradient was applied to the same cells by a micropipette filled with 0.1 μM cAMP. After image acquisition in the absence of the cAMP stimulus, the micropipette was positioned manually. Fluorescence data were not obtained during this operation.

Microscopy

Confocal imaging was performed by inverted microscopes (TiE, Nikon, Japan) equipped with a spinning disk confocal unit (CSU X1, Yokogawa, Japan). $PH_{Akt/PKB}$-EGFP was excited by 488 nm solid-state lasers. Fluorescence images were acquired by EMCCD camera (iXon+, Andor, Belfast, Northern Ireland). Images of $PH_{Akt/PKB}$-EGFP expressing cells were taken every 3 s. The cAMP stimulation was performed using a micropipette (FemtoTips, Eppendorf, New York) filled with cAMP and Alexa 555, pressurized at 100 hPa using an injector (FemtoJet, Eppendorf). The formation of the cAMP spatial gradient was confirmed by dye imaging. Image analysis was performed using Matlab (Mathworks, Natick, MA).

The theoretical model

The state of the system is described by the membrane concentrations of PtdIns(3,4,5)P3 (P_3), PtdIns(4,5)P2 (P_2), membrane PTEN (E), and cytosol PTEN (E_c), denoted by P_3, P_2, E, and E_c, respectively. The reaction kinetics and their rates were described previously (21,23).

	Reactions	*Rates*
1	$P_3 \rightarrow P_2$	$V_1 E \frac{P_3}{K_1 + P_3}$
2	$P_2 \rightarrow P_3$	$V_2 a \frac{P_2}{K_2 + P_2}$
3	$P_3 \rightarrow$	$\lambda_3 P_3$
4	$\rightarrow P_2$	k
5	$P_2 \rightarrow$	$\lambda_2 P_2$
6	$E_c \rightarrow E$	$V_{ass} E_c \frac{K_4}{K_4 + P_3} \frac{P_2}{K_5 + P_2}$
7	$E \rightarrow E_c$	$\lambda_E a E$

Here, V_1, K_1, V_2, K_2, λ_3, k, λ_2, V_{ass}, K_4, K_5, and λ_E are reaction constants. Reactions 1 and 2 are the enzymatic reactions of PTEN and PI3K, respectively. Reactions 3 and 5 are the degradation reactions. Reaction 4 is a supply reaction for P_2. Reactions 6 and 7 are the membrane association and dissociation reactions of PTEN. The association rate depends on both concentrations of P_3 and P_2 as described previously (23). Reactions 2 and 7 depend on the chemoattractant stimulus, where the parameter a describes the chemoattractant-dependent membrane activity. Under linear gradients with $\Delta\%$ steepness in the cell length (diameter $2R$), we supposed that $a = a(\theta)$ is given by

$$a(\theta) = 1 + \frac{\Delta}{100}\frac{1}{2}\cos\theta. \quad (1)$$

The diffusion constants in the cytosolic region are much faster than the diffusion constants on the plasma membrane (for PTEN, see 30,31). Because of this fast diffusional transport in the cytosol, the cytosol concentration of E is approximately given by $E_c = E_t - \chi\bar{E}$, where E_t is the total concentration of E, $\bar{E}$ is the instantaneous space average of E, and χ is the constant used to change the membrane to the cytosol concentrations. Diffusional transport on the plasma membrane is included for P2 and P3 with diffusion constant D_P, and E with D_E. For the parameter values, we used the same value of the previous reports (21,23), which are indicated in the figure legends.

All simulations were performed using a stochastic algorithm. For convenience, we show the differential equation corresponding to the above reaction scheme as

$$\frac{\partial P_3}{\partial t} = -V_1 E \frac{P_3}{K_1 + P_3} + V_2 a(\theta) \frac{P_2}{K_2 + P_2} - \lambda_3 P_3 + D_E \Delta P_3 \quad (2)$$

$$\frac{\partial P_2}{\partial t} = V_1 E \frac{P_3}{K_1 + P_3} - V_2 a(\theta) \frac{P_2}{K_2 + P_2} + k - \lambda_2 P_2 + D_P \Delta P_2 \quad (3)$$

$$\frac{\partial E}{\partial t} = V_{ass} E_c \frac{K_4}{K_4 + P_3} \frac{P_2}{K_5 + P_2} - \lambda_E a(\theta) E + D_E \Delta E. \quad (4)$$

For wave sensing, we introduced an adaptation motif upstream of the PtdIns lipid reaction. We did not aim to present a model that accounts for

the detailed biochemistry of the adaptation motif, but rather one that captures the essential characteristics of spatial and temporal behaviors of the modulation in the PtdIns lipid signaling reaction. When a concentration wave of chemoattractant is present, for the membrane activity $a(\theta)$, we considered the following differential equation:

$$\begin{aligned}\frac{\partial a(\theta,\mathrm{t})}{\partial t} &= \frac{1}{\tau}\left(\frac{c(\theta,t)}{\overline{b(t)}} - a(\theta,t)\right)\\ \frac{\partial b(\theta,\mathrm{t})}{\partial t} &= c(\theta,t) - b(\theta,t)\end{aligned} \tag{5}$$

where $a(\theta,t)$, $b(\theta,t)$, and $c(\theta,t)$ are the membrane activity, an additional variable and the chemoattractant concentration at position θ and time t, respectively (32). In the first equation, $\overline{b(t)}$ is the average of $b(\theta,t)$ with respect to the position θ at a given time t. The wave of chemoattractant concentration was given by

$$c(\theta,t) = c_0 + c_1\frac{e^{\mu\,\cos[2\pi(t/T - x(\theta)/X)]} - e^{-\mu}}{e^{\mu} - e^{-\mu}}, \tag{6}$$

with

$$x(\theta) = R\cos(2\pi\theta),$$

where c_0 and c_1 are the minimum and maximum concentrations, respectively; μ determines the steepness of the gradient; T and X give the time and space period of the wave, respectively; and R is the radius of the cell.

Numerical simulations

For numerical simulations, we studied a one-dimensional system along the membrane. The radius of the cells, R, was set at 5 μm, which is typical for latrunculin A treated cells. For the stochastic simulation, we used the Estimated-Midpoint τ-leap Method (33) with 100 grids and a constant time step $\Delta t = 0.0005$ s. To obtain the concentration at each grid, the molecular numbers were divided by the grid size Δx (μm) or $1 \times \Delta x$ (μm^2). For the numerical simulation in Eq. (5), we used the implicit Euler scheme with the same constant time step $\Delta t = 0.0005$ s.

The precision of domain formation

In Fig. 3 *D*, the precision of domain formation was characterized by the inverse of the circular standard deviation. The circular standard deviation is given by $\sigma_D = \sqrt{-2\log R}$ with $R = \sqrt{\overline{\cos\theta}^2 + \overline{\sin\theta}^2}$, where θ is the direction of domain and the over line indicates the statistical average.

RESULTS

Gradient responses of *Dictyostelium* cells

We studied the response of the PtdIns lipid system to extracellular cAMP gradient by monitoring the distribution of PtdIns(3,4,5)P3 using the EGFP-labeled PH-domain of Akt/PKB (PH-GFP). In Fig. 1 *A*, we showed the responses of cells treated with 4 mM caffeine to inhibit cell-to-cell

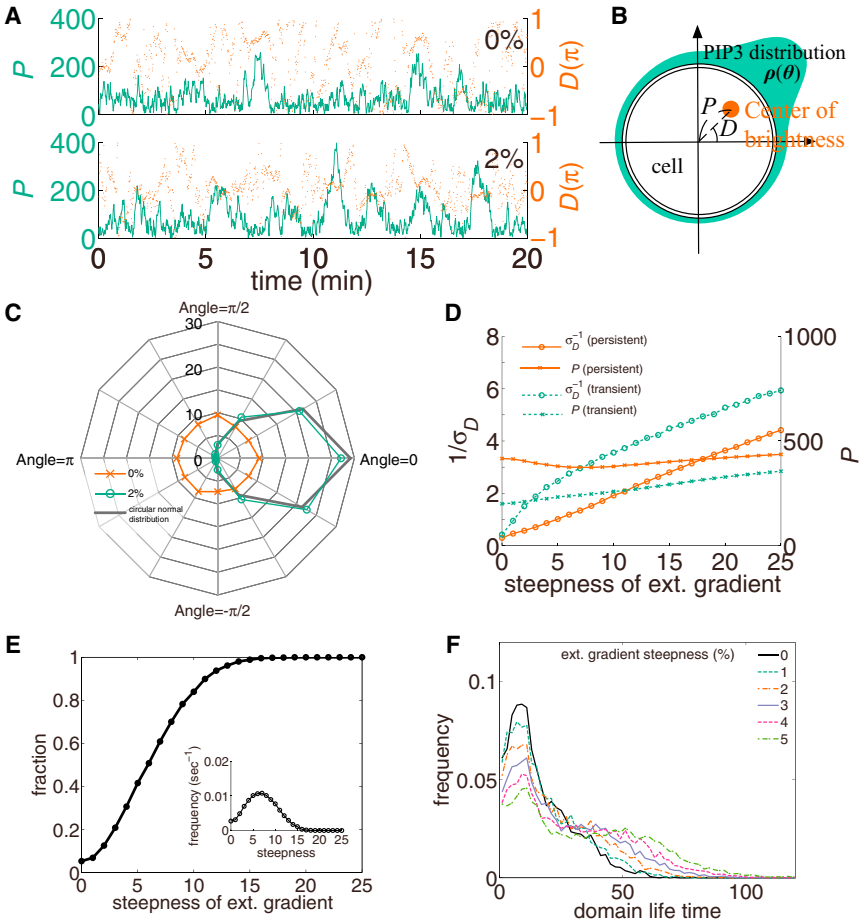

FIGURE 3 Responses of the transiently formed domain to external gradient. (*A*) Time series of domain formation in the case of spontaneous transient domain formation for 0% and 2% external gradients. Green and red lines indicate the amplitude P and angle D, respectively, of the center of [PIP3] distribution along membrane. (*B*) Schematic diagram of center of PtdIns(3,4,5)P3 distribution. The circle indicates a cell. At each angle θ on membrane, PtdIns(3,4,5)P3 concentration is a function of θ, $\rho(\theta)$, which is schematically indicated by green around the cell. The amplitude P and angular direction D are in polar coordinates, which are defined as $Pe^{iD} = \oint\rho(\theta)e^{i\theta}d\theta$. (*C*) The distribution of domain position for 0% (*red*) and 2% (*green*) gradients. We considered that domains were formed when P crosses the threshold from lower to larger values of the threshold (150). Gray line is the circular normal distribution with the concentration parameter 2.27. (*D*) The inverse of the circular standard deviation of angle D around the average $D = 0$ and the average of amplitude P of the center plotted against the steepness of the external gradient. (*E*) Fraction of time that P is larger than the threshold value (150) plotted against the steepness of the external gradient. Insert shows the frequency that P crosses the threshold from lower to larger values plotted against the steepness. (*F*) Distribution of the time duration that P is larger than the threshold value (150) for different steepness values.

interactions via secreted cAMP. A PH-GFP–enriched domain was persistently produced as reported previously (21). In the absence of a chemoattractant (cAMP) gradient, the domain showed a traveling motion. When a cAMP gradient was applied, the domain position was biased along the gradient. Interestingly, the domain kept its traveling motion within a restricted region and exhibited zigzag patterns. In Fig. 1 *B*, we showed the responses of cells without caffeine treatment. In the absence of gradient (Fig. 1 *B*, left), a PH-GFP–enriched domain were formed transiently at a random position as has been reported previously (18,23). We then applied gradients to the same cells using a micropipette containing cAMP (see Materials and Methods). When a gradient was applied, the PH-GFP-enriched domain was oriented to the source of cAMP, as has been well documented in previous studies (34). Interestingly, the domains under gradients were formed still transiently. In these cases, we found that the gradient responses still retain the properties of spontaneous domain formations, even in the presence of gradient.

It has been demonstrated quantitatively that very shallow gradients with a few percent of steepness in the cell length can induce chemotaxis, and the chemotaxis accuracy increases with the steepness of gradient (35). With the self-organization activities in this chemotaxis signaling system, how do cells achieve such high sensitivity, and how does the steepness information quantitatively modulate the intracellular processes so that the chemotaxis accuracy increases with the steepness? Motivated by the observations, in the following sections, we develop a mathematical model to study theoretically the gradient response of the self-organization system.

Modeling gradient response by self-organized PtdIns lipid signaling

To elucidate the mechanism for highly sensitive gradient sensing, we studied a model of self-organized formation of PtdIns(3,4,5)P3–enriched domains (23).We introduced chemoattractant-dependent regulations into the model that was published previously to explain the spontaneous activity of this singling reaction (21,23). The reaction scheme was based on the cyclic phosphorylation and dephosphorylation of PtdIns(4,5)P2 and PtdIns(3,4,5)P3, the attachment and detachment of enzymes from the membrane, and diffusional transport of the lipids and enzymes through both membrane and cytosol (Fig. 2 *A*; Materials and Methods). We also considered chemoattractant-dependent effects in the phosphatidylinositol lipid reaction. We first considered PI3K membrane activity to be dependent on the stimulus (dotted line (a) in Fig. 2 *A*). The activity of PI3K, probed by the PtdIns(3,4,5)P3–binding domain, exhibits adaptation kinetics for step-wise increases of cAMP concentration (36,37). Situated in a gradient, PI3K shows localized activity only at the leading edge of the cell. Recently, a network motif upstream of PI3K that includes Ras was found to show adaptation kinetics in response to step-wise increases in a chemoattractant stimulus (38). Theoretically, when within a gradient, a cell's adaptation kinetics with a cell global regulator can produce an intracellular gradient of activity in which the activity is elevated from baseline at one side, lower than baseline at the other side, and almost the same as the baseline level in the middle region of cell. This space and time characteristic has been proposed to be explained by the LEGI model (39,40). Therefore, in our model, the membrane PI3K activity in the region facing the higher chemoattractant concentration is supposed to be higher than the baseline level, and activity on the other side to be lower than baseline (see Materials and Methods for mathematical expressions). PTEN shows membrane unbinding in response to the stimulus, even without PI3K (41), and it shows localization at the region of the membrane facing the lower end of the gradient (42). Thus, we supposed that PTEN affinity for the membrane is also dependent on the chemoattractant, similarly to but independent of PI3K (dotted line (b) in Fig. 2 *A*; see Materials and Methods).

Sharp response to an external gradient in self-organized PtdIns reaction

As mentioned in Introduction, in the absence of gradient, this model exhibits three types of behaviors: 1) quiescent state, 2) transient domain formation, and 3) persistent domain formation. In Fig. 2 *B–D*, the responses to 1% to 10% external gradients were plotted with time for the three cases described above. For all cases, internal gradients of PtdIns(3,4,5)P3 were generated. The time-average of the spatial profiles of PtdIns(3,4,5)P3 concentration under 5% external gradients are plotted in Fig. 2 *E*. The dependence of the internal gradient on the external gradient is shown in Fig. 2 *F*. When a gradient was applied to the quiescent state (first case) as shown in Fig. 2 *B*, an internal gradient was produced, but it was shallow and membrane accumulation of PtdIns(3,4,5)P3 was not obvious (Fig. 2 *E*, blue). The average steepness of the internal gradient increased linearly in proportion to the steepness of the external gradient (Fig. 2 *F*, blue). The steepness of the internal gradient was larger than the external gradient, indicating the presence of an amplification effect, even in this case. In contrast, when the PtdIns(3,4,5)P3 domains formed spontaneously, either transiently or persistently (Fig. 2 *D* and *C*), the spontaneously formed domains were distributed along the external gradient. The averaged spatial profile of PtdIns(3,4,5)P3 was much steeper than in the case without spontaneous domain formation (Fig. 2 *E*, green and red), indicating that the self-organized domain formation plays a positive role in sensing the gradient. In the case of transient domain formation, for steep gradients, domains are persistently formed on the membrane region facing the higher chemoattractant concentration. The increase in average internal

steepness in relation to the external steepness could be caused by increases in PtdIns(3,4,5)P3 concentration in individual domains, precision of domain position, or frequency of domain formation.

Gradient steepness is encoded in accuracy and frequency of domain formation

We next focused on the case in which domains are formed transiently (second case, Fig. 2 *C*), that is, PtdIns(3,4,5)P3–enriched domains are repeatedly formed with finite lifetimes, even in the presence of extracellular gradient, as was observed experimentally (Fig. 1 *B*, left).

To quantitatively characterize the domain formation in the absence and presence of a gradient, we plotted the time series of the center of the PtdIns(3,4,5)P3 distribution (Fig. 3 *A*). The center is given by the amplitude P and angle D in polar coordinates (defined as $Pe^{iD} = \oint \rho(\theta) e^{i\theta} d\theta$, where $\rho(\theta)$ is the concentration of PtdIns(3,4,5)P3 on the membrane at angle θ (see Fig. 3 *B*)). The external gradient was directed to $\theta = 0$. Here, P indicates the asymmetry degree in the PtdIns(3,4,5)P3 distribution and D is its direction. When PtdIns(3,4,5)P3 is distributed uniformly, P is zero and D shows no defined direction. As shown in Fig. 3 *A*, when a domain is formed, P increases (green) and the temporal fluctuation of direction D is reduced (red). We see that domain formation is a stochastic process. Without an external gradient, the positions of formed domains are randomly distributed, whereas under the 2% gradient, the positions of formed domains are biased toward the direction of the gradient ($D = 0$).

In Fig. 3 *C*, we plotted the distributions of D at the time when a domain was formed (P rose above a given threshold value). When there was no gradient, the position of the domain formation was distributed uniformly (Fig. 3 *C*, red). In contrast, for a 2% gradient, the position of the domain formations was sharply distributed around the direction of the gradient (Fig. 3 *C*, green).

Next we studied the dependence of the position precision on the steepness of the external gradient (Fig. 3 *D*, blue circle). The precision can be characterized by the inverse of the circular standard deviation of domain position D, which increases with steepness (see Materials and Method for calculation). In contrast, the polarity intensity P was relatively constant, indicating that this domain property is less affected by the external gradient. Next, we studied the frequency of domain formation, as measured by the fraction of total time during which domains were forming (Fig. 3 *E*). This fraction increases with the steepness of the external gradient. The frequency of domain formation also increases, for gradients up to 7% (Fig. 3 *E,* inset). In contrast, the lifetime of individual domains shows a small dependence on the steepness, with a lifetime of ~10 s to one min (Fig. 3 *F*). Therefore, the increase in the average steepness of the intracelluar gradient results from an increase both in spatial precision and temporal frequency modulation rather than an increase in the PtdIns(3,4,5)P3 instantaneous intensity. On the contrary, the PtdIns(3,4,5)P3 intensity is an intrinsic property of the PtdIns lipid reaction, which is thus almost independent of guidance cues.

Taken together, our results indicate that in gradient sensing by self-organization systems, information about the external gradient is spatially encoded in the position precision of signaling domains and temporally encoded in the frequency of signaling domain formation. As gradient steepness further increases, the time interval between the domain formations is reduced and domains are persistently formed on the membrane subjected to higher chemoattractant concentration. Therefore, the internal steepness increased rapidly with the external steepness for shallow gradients and showed saturation at an extracellular gradient of ~15% (i.e., external steepness did not lead to further internal steepness; Fig. 2 *F*, green and red).

Our model includes chemoattractant-dependent and PtdIns(3,4,5)P3-independent regulation of both PI3K and PTEN (lines (a) and (b) in Fig. 2 *A*). When we included chemoattractant-dependent regulation of PI3K (lines (a) in Fig. 1 *C*) but not of PTEN (without line (b) in Fig. 2 *A*)) in the model, the domain position was biased toward the gradient direction as shown in Fig. 4 *A*. The relative steepness of the PtdIns(3,4,5)P3 gradient formed on the membrane also showed the same characteristics (Figs. 4 *B*). Its saturation level was almost the same (Figs. 4 *B* and 2 *E*), although the relative steepness reaches saturation at a steeper external gradient than in the double-regulation case. The frequency

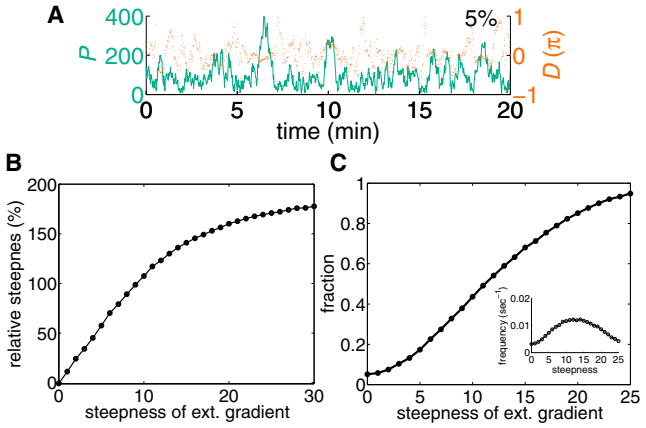

FIGURE 4 Gradient response without chemoattractant-dependent regulation on PTEN. Here, we consider that only the total activity and concentration of PI3K on membrane is dependent on the chemoattractant stimulus (dotted line (a) in Fig. 2 *A*), but PTEN is independent of the chemoattractant. In the absence of a gradient, the transient domain of PtdIns(3,4,5)P3 is formed as shown in Fig. 3 *A* (*top*). (*A*) Time series of domain formation for 5% external gradients. (*B*) Relative steepness in [PIP3] is plotted against the external steepness. (*C*) Fraction of time that P is larger than the threshold value (150) plotted against the steepness of the external gradient. Insert shows the frequency that P crosses the threshold from lower to larger values plotted against the steepness.

of domain formation also increases with the steepness of the external gradient (Fig. 4 *C*). Thus, the gradient response was qualitatively the same in both cases. Once a domain is formed, its properties are inherently determined.

The threshold for domain formation is polarized along the gradient

As shown in Fig. 3 *C* (green), the frequency of PtdIns(3,4,5)P3–enriched domain formation is higher at the anterior region facing the higher concentration of chemoattractant. In Fig. 5 *A*, we plotted the probability that a local membrane region of a particular PtdIns(3,4,5)P3 concentration (horizontal axis) at a time shows a domain formation, both without a gradient (cross) and with a gradient (anterior side (circle), lateral side (asterisk), posterior side (plus sign). The concentration at which the probability of domain formation reaches 0.5 is lower at the anterior region in the presence of a gradient (circle) than it is without a gradient (cross). On the contrary, such concentration is larger at the posterior region with a gradient (plus sign) than without a gradient (cross). This indicates that the PtdIns(3,4,5)P3 concentration leading to a domain formation is lower in the anterior region, and this region thus shows more frequent domain formation.

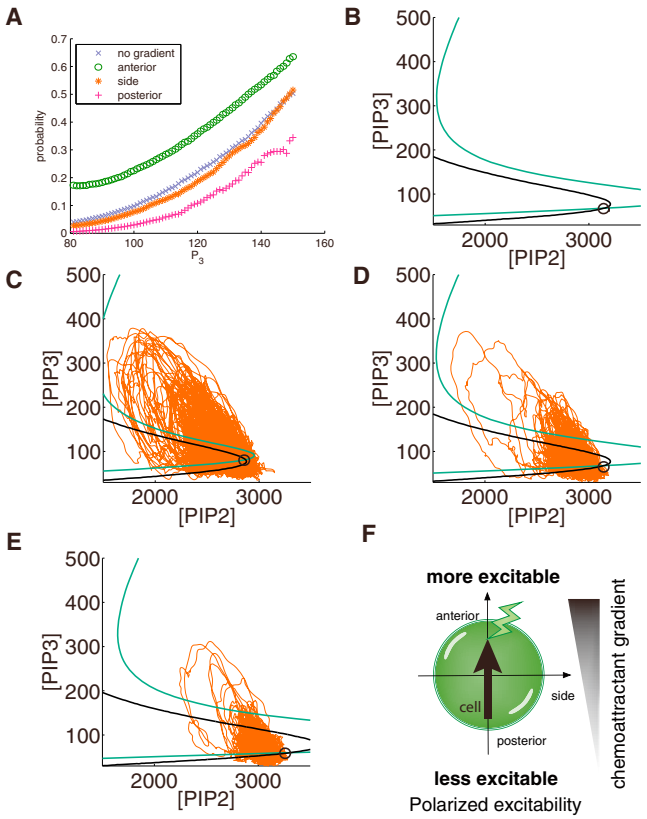

FIGURE 5 Modulation of the threshold for domain formation along gradient. (*A*) The probability that the state reaching P_3 resulted in the formation of a domain in the absence of a gradient (*blue*) or in the presence of a 2% gradient (higher concentration side, *green*; lateral side, *red*) Here, we calculated for a membrane region with a given value of $P_3(0)$ at a given moment (t=0), the probability that $P_3(t)$ reached and exceeded a given threshold value (excitation; $P_3 = 180$) before returning to the initial value $P_3(0)$. The result was not qualitatively dependent on the threshold value. (*B*) Null-clines for $dP_2/dt = 0$ (*black*) and $dP_3/dt = 0$ (*green*) for the situation without gradient. The ordinary differential equation is given by Eqs. (2), (3) and (4) without the diffusion term. Here, E in Eqs. (2) and (3) was adiabatically eliminated by substituting a function $E = E(P_3, P_2)$, which was obtained by solving $dE/dt = 0$ in Eq. (4), into Eqs. (2) and (3). (*C–E*) Null-clines for the situation with 2% gradient (*C*: *anterior*, *D*: *lateral*, *E*: *posterior*). The trajectories in the corresponding regions are shown in red. (*F*) Schematic diagram of polarized excitability.

To see the difference in the threshold level along the gradient, we studied the interdependence between the concentrations of PtdIns(4,5)P2 and PtdIns(3,4,5)P3. Let P_2 and P_3 be the concentrations, respectively. In Fig. 5 *B*, we plot the "null-clines" on which the rate of change in P_2 or P_3 vanishes: $dP_2/dt = 0$ and $dP_3/dt = 0$ (black and green, respectively.) When P_2 or P_3 passes across the null-clines, one of the concentrations exhibits a change from an increase to a decrease, or the opposite. At the crossing point of two lines, the two concentrations are stationary without changes (open circle in Fig. 5 *B*). When a small perturbation is applied to P_3 not to cross the null-cline given by $dP_3/dt = 0$ (green line in Fig. 5 *B*), the concentrations quickly return to the stationary state (open circle in Fig. 5 *B*). However, if the perturbation is sufficiently large for P_3 to cross the null-cline, P_3 shows a further increase until it turns to decreasing again. Thus, the null-cline creates a threshold. Such an autonomous change away from the stationary state until it starts returning to the stationary state is a characteristic behavior of excitable systems.

As the distance from the stationary state to the threshold decreases, the reaction becomes more susceptible to excitation in response to small perturbations. Because the production rate of PtdIns(3,4,5)P3 and the membrane affinity of PTEN are dependent on the position along the membrane, the distance to the threshold can also depend on the position along the membrane. In Fig. 5 *C–E*, the null-clines are plotted for three different points along the membrane. Along the gradient from posterior to anterior regions, the distance from the stationary state to the null-clines decreases, indicating that the state is more excitable in the anterior region than the posterior region. The red lines are the traces of two concentrations obtained at the corresponding three regions; the anterior region is indeed more excitable than the posterior region. In summary, under a gradient, the excitability is polarized in a manner such that the anterior region is more excitable than the posterior region (polarized excitability; Fig. 5 *F*).

In the null-cline analysis, the effects of diffusional transport are excluded. However, the diffusion through the cytoplasmic region can give rise to interactions among different membrane regions. For instance, the formation of PtdIns(3,4,5)P3 domains leads to an increase in the cytosol PTEN concentration and consequently a change in the

reaction kinetics of entire membrane regions. The result is a reduction in the possibility for additional domain formation and thus an increase in the probability of single domain formation.

Gradient sensing by persistently formed domains

We next study the third case when domains are persistently formed by self-organization (Fig. 2 *C*). Under external gradients, the domain still exhibits some motion. As the steepness of an external gradient increases, the domain motion is restricted at the high external concentration side. The domain travels in a direction until a particular position, at which point the domain changes its direction and returns to the opposite direction. Repeating this process, the domain motion exhibits a kind of zigzag pattern. This pattern is similar to the experimental observation shown in Fig. 1 *A*. Thus, the domain probability increases at the high-concentration side along the gradient. The position precision of the domain gradually increases with the increase in external steepness (Fig. 3 *D*, red circle), whereas the polarity intensity P changes slightly. Therefore, for gradient sensing, the PtdIns(3,4,5)P3 domain position is biased toward the direction of the gradient, and the degree of bias increases with the increase in steepness.

Wave sensing in the combined system of adaptive and excitable motifs

So far, we have shown that the self-organizing signaling system exhibits sharp responses to shallow gradients. We also showed that the gradient sensing works by modulating the threshold for generating self-organizing signaling domains. One possible role of such a system is wave sensing. *Dictyostelium* cells have been known to show directional migrations in response to the concentration waves of cAMP (33). Because waves consist of both positive and negative gradients to the direction of motion, how cells can migrate toward the center of waves has been debated (44,45). A refractoriness of the signaling pathway after a cAMP concentration increase is one possible mechanism (44,45). Here, we consider a different mechanism of wave detection, which is performed by the combined system consisting of adaptive and excitable motifs.

In *Dictyostelium* cells, it has been demonstrated that a temporal increase and decrease in cAMP concentration induces increases and decreases in Ras activity, respectively, which then returns to the baseline level (38). Such adaptation kinetics underlie the detection of temporal changes in a stimulus, as in the case of bacterial chemotaxis (46), and the network motif including Ras in *Dicsyostelium* cells operates similarly. In the present model of PtdIns lipid signaling, Ras activity can modulate PI3K activity. According to the results described in the previous section, an increase and decrease in Ras activity probably decreases and increases the threshold value for domain formation, respectively. Combining the responses of Ras to cAMP and PtdIns(3,4,5)P3 to Ras activity, the temporal increase and decrease in the cAMP stimulus increases and decreases the probability of PtdIns(3,4,5)P3–enriched domain formation.

To demonstrate this idea, we introduced in the present model a simple adaptive motif that changes both PI3K membrane activity and PTEN membrane affinity (Fig. 2 *A*; see Materials and Methods in detail). Thus, the model is similar in its mathematical essence to the LEGI-excitable model (28). We performed numerical simulations for stimuli that are spatially uniform and temporally either increasing or decreasing, as shown in Fig. 6 *A* and *B*. The result clearly indicates that the PtdIns(3,4,5)P3–enriched domain was formed only when the stimulus increased with time, demonstrating that the threshold for domain formation can be modulated by temporal signals. We then applied stimulus waves to the model. Fig. 6 *C* shows the space and time concentrations of PtdIns(3,4,5)P3 and cAMP (top and bottom, respectively) and the cAMP concentrations at $\theta = 0$ and $\theta = \pi$ (red and yellow lines, respectively). The PtdIns(3,4,5)P3–enriched domain formed and was appropriately oriented when the cell experienced positive gradients with temporal increase, but this was not seen for negative gradients with temporal decrease. When the wave speed is too fast, cells cannot respond. When the wave speed is too slow, the domain is formed in both directions, with positive and negative steepness (Fig. 6 *D*). In conclusion, to sense the spatial direction of stimulus waves, the adaptive motif detects the temporal change in the stimulus, which is then transduced into spatial information by the excitable motif, in the combined system. The property of the sharp asymmetry formation of excitable motif provides a robust way for wave sensing.

DISCUSSION

In our model, the self-organizing signaling system produces a sharp intracellular asymmetry in the distribution of signaling molecules, which is independent of extracellular guidance cues. Extracellular guidance cues modulate the property of excitability at localized membrane regions. The membrane region in contact with higher chemoattractant concentrations is more excitable than the other regions. The sharp response to shallow gradients is thus made possible by this biased excitability mechanism (Figs. 2 and 5). For a given steepness, the direction of the signaling domain is distributed according to a circular normal distribution (Gaussian distribution on a circle; Fig. 3 *C*), indicating that the dynamics of domain direction can be described by a relatively simple stochastic process. Once a domain position is determined, a sharp internal gradient is produced by the self-organizing process. The sharpness in the gradient response is intrinsic to the self-organizing

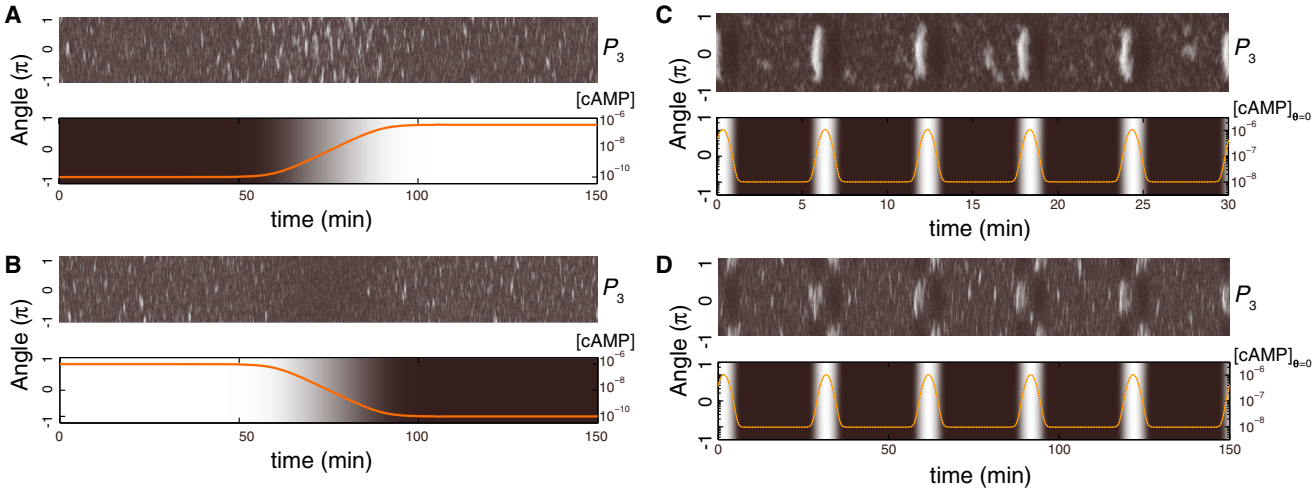

FIGURE 6 Wave sensing in the system with adaptive and excitable motifs. (*A–B*) The responses of PtdIns(3,4,5)P3 (*top panel*) for spatially uniform and temporally increasing (*A*) and decreasing (*B*) stimuli (*bottom panel*). The concentrations were increased and decreased from $c_0 = 10^{-8}$ to $c_1 = 10^{-6}$ and vice versa during 30 min. (*C–D*) The responses of PtdIns(3,4,5)P3 for waves with a period of 6 min (*C*) and 30 min (*D*). Temporal changes in the stimulus intensity occur first at the anterior region (angle $\theta = 0$), and they are delayed from anterior to posterior (from $\theta = 0$ to 180°), as shown in the bottom panels. Red solid and yellow dotted lines show the cAMP concentrations at $\theta = 0$ and $\theta = 180°$, respectively. For the excitable motif, the parameter values are given in Fig. 2 *B*. For the adaptive motif, $\tau = 1$ sec. For the wave, we used $c_0 = 10^{-8}$M, $c_1 = 10^{-6}$M and $\mu = 15$ with periods $T = 6$ min., $X = 3$mm (C) and $T = 30$ min., $X = 15$mm (D). Here, we determined the wave parameter values based on the previous report (43).

reaction and mostly independent of the external gradient. Thus, the sharp response, as shown in Fig. 2 *E*, can be understood as a convolution of the domain position establishment by a simple stochastic process and the sharp domain formation by a nonlinear self-organizing process.

The localized signaling domain for gradient sensing should exhibit reasonable responsiveness and readjustment for directional changes in the external gradient, without showing too much positional persistence. With these characteristics, the domain is more capable of exhibiting wave-like behavior or transient formation with repeated creation and annihilation (25). The PtdIns(3,4,5)P3–enriched domain actually has this characteristics as shown in both mathematical model and experimental observation (Figs. 1 and 2).

Signals upstream of PtdIns lipids reactions are noisy (2). To extract gradient information from the noisy signal, the characteristic time of the localized signaling domain should be slower than the time constants of noise in upstream signals (3). The signaling domain produced by self-organization can work as an emergent parameter that stores directional information, which can be controlled by external gradients. Self-organization with spontaneous symmetry breaking provides such a macro parameter, which varies slowly, is controllable by external signals. Because slow parameters can average out fast fluctuations according to the law of large numbers, the signaling domain with symmetry breaking state has robustness against extra- and intracellular noise (47). These properties are important for robust gradient sensing. Because the PtdIns lipid signaling pathway shows this characteristics, this pathway among several parallel pathways is particularly indispensable for robust chemotaxis in a shallow chemoattractant gradient. Our results are naturally seen in many excitable systems, although our present analysis was based on a particular mathematical model.

Signals generated by self-organization could also be effective in downstream processes. Because PtdIns(4,3,5)P3 induces directional cell migration, molecular processes in the motile activity such as cytoskeletal reorganization should be coordinately activated. If the signal intensity (the concentration of PtdIns(4,3,5)P3) increased quantitatively with external gradient steepness, then the weak signal generated under shallow gradients would lead to activation of some processes that have threshold values lower than the signal intensity but not others with threshold values larger than the signal intensity. As a result, coordinated production of motile activity would become complicated. However, based on our results with the self-organization mechanism, the PtdIns(3,4,5)P3 concentration in the localized domain is almost independent of the steepness of the external gradient. Even in a shallow gradient, although the domain position may not be accurate, the signal in a localized domain could have an intensity sufficiently larger than the activation threshold of most of the downstream processes. As a result, the activation of a variety of downstream processes could take place synchronously and thus motile activities could be produced without the need for complicated coordination. Therefore, it could be natural that the external gradient steepness modulates the domain precision and frequency to increase chemotaxis accuracy. Such a mechanism enables a signaling system to internally discriminate the external gradient steepness.

In this study, the polarization in the excitability was explained by the modulation in the threshold for excitation at individual membrane regions along the cell body. In the membrane region in contact with higher chemoattractant concentrations, the threshold of signaling level for domain formation is lower than the other regions. As mentioned, the diffusional transport through membrane and cytoplasmic region may also play a role for the preferential activation along the gradient. More elaborated mathematical analysis is necessary to elucidate the role of these effects for the sensitive response to shallow gradients.

Previous studies have shown that the cell motility exhibits persistence without much change in direction for a few minutes, implying that the cells have some directional memory (10–12). The responsiveness for chemoattractant is also reported to show a kind of memory effect in well-elongated cells; the anterior region shows a quicker response than the posterior region (48). With the present results, these observations may be related to polarized excitability that is established independent of extracellular guidance cues.

CONCLUSION

In this paper, we studied theoretically the response of self-organizing system to guidance cues. Our analysis indicated that self-organized signaling domains respond sharply to a shallow external gradient by increasing the precision of polarity direction and modulating the frequency of self-polarization. External guidance cues modulate the probability of domain formation by changing the threshold for domain formation along gradients. All these results indicate that self-organizing activity, independent of external cues, is the basis for the sharp responses to shallow gradients. By combining with adaptive motif, such threshold regulation can also work to sense sharply directional signals from spatially and temporally changing stimulus waves.

We thank Hiroaki Takagi, Tetsuya Hiraiwa, Katsuhiko Sato, Naotoshi Nakamura and the members of Laboratory for Physical Biology in RIKEN CDB and Cell Signaling Dynamics group in RIKEN QBiC for generous discussion.

This work was supported by grant-in-aid (KAKENHI) from MEXT [grant number 23111531 to T.S. and 22111002 to M.U.].

REFERENCES

1. Bray, D. 2001. Cell movements: from molecules to motility, 2nd ed. Garland, New York.
2. Ueda, M., and T. Shibata. 2007. Stochastic signal processing and transduction in chemotactic response of eukaryotic cells. *Biophys. J.* 93:11–20.
3. Shibata, T., and K. Fujimoto. 2005. Noisy signal amplification in ultrasensitive signal transduction. *Proc. Natl. Acad. Sci. USA.* 102:331–336.
4. Swaney, K. F., C. H. Huang, and P. N. Devreotes. 2010. Eukaryotic chemotaxis: a network of signaling pathways controls motility, directional sensing, and polarity. *Annu Rev Biophys.* 39:265–289.
5. Veltman, D. M., I. Keizer-Gunnik, and P. J. Van Haastert. 2008. Four key signaling pathways mediating chemotaxis in Dictyostelium discoideum. *J. Cell Biol.* 180:747–753.
6. Kortholt, A., R. Kataria, …, P. J. Van Haastert. 2011. Dictyostelium chemotaxis: essential Ras activation and accessory signalling pathways for amplification. *EMBO Rep.* 12:1273–1279.
7. Van Haastert, P. J., and P. N. Devreotes. 2004. Chemotaxis: signalling the way forward. *Nat. Rev. Mol. Cell Biol.* 5:626–634.
8. Welf, E. S., S. Ahmed, …, J. M. Haugh. 2012. Migrating fibroblasts reorient directionality by a metastable, PI3K-dependent mechanism. *J. Cell Biol.* 197:105–114.
9. Sasaki, A. T., C. Janetopoulos, …, R. A. Firtel. 2007. G protein-independent Ras/PI3K/F-actin circuit regulates basic cell motility. *J. Cell Biol.* 178:185–191.
10. Takagi, H., M. J. Sato, …, M. Ueda. 2008. Functional analysis of spontaneous cell movement under different physiological conditions. *PLoS ONE.* 3:e2648.
11. Li, L., E. C. Cox, and H. Flyvbjerg. 2011. 'Dicty dynamics': Dictyostelium motility as persistent random motion. *Phys. Biol.* 8:046006.
12. Bodeker, H. U., C. Beta, …, E. Bodenschatz. 2010. Quantitative analysis of random ameboid motion. *Europhys. Lett.* 90:28005.
13. Killich, T., P. J. Plath, …, M. G. Vicker. 1993. The locomotion, shape and pseudopodial dynamics of unstimulated Dictyostelium cells are not random. *J. Cell Sci.* 106:1005–1013.
14. Vicker, M. G. 2000. Reaction-diffusion waves of actin filament polymerization/depolymerization in Dictyostelium pseudopodium extension and cell locomotion. *Biophys. Chem.* 84:87–98.
15. Gerisch, G., T. Bretschneider, …, K. Anderson. 2004. Mobile actin clusters and traveling waves in cells recovering from actin depolymerization. *Biophys. J.* 87:3493–3503.
16. Weiner, O. D., W. A. Marganski, …, M. W. Kirschner. 2007. An actin-based wave generator organizes cell motility. *PLoS Biol.* 5:e221.
17. Asano, Y., A. Nagasaki, and T. Q. Uyeda. 2008. Correlated waves of actin filaments and PIP3 in Dictyostelium cells. *Cell Motil. Cytoskeleton.* 65:923–934.
18. Postma, M., J. Roelofs, …, P. J. Van Haastert. 2004. Sensitization of Dictyostelium chemotaxis by phosphoinositide-3-kinase-mediated self-organizing signalling patches. *J. Cell Sci.* 117:2925–2935.
19. Postma, M., J. Roelofs, …, P. J. Van Haastert. 2003. Uniform cAMP stimulation of Dictyostelium cells induces localized patches of signal transduction and pseudopodia. *Mol. Biol. Cell.* 14:5019–5027.
20. Weiger, M. C., C. C. Wang, …, J. M. Haugh. 2009. Spontaneous phosphoinositide 3-kinase signaling dynamics drive spreading and random migration of fibroblasts. *J. Cell Sci.* 122:313–323.
21. Arai, Y., T. Shibata, …, M. Ueda. 2010. Self-organization of the phosphatidylinositol lipids signaling system for random cell migration. *Proc. Natl. Acad. Sci. USA.* 107:12399–12404.
22. Bosgraaf, L., I. Keizer-Gunnink, and P. J. Van Haastert. 2008. PI3-kinase signaling contributes to orientation in shallow gradients and enhances speed in steep chemoattractant gradients. *J. Cell Sci.* 121:3589–3597.
23. Shibata, T., M. Nishikawa, …, M. Ueda. 2012. Modeling the self-organized phosphatidylinositol lipid signaling system in chemotactic cells using quantitative image analysis. *J. Cell Sci.* 125:5138–5150.
24. Iglesias, P. A., and P. N. Devreotes. 2008. Navigating through models of chemotaxis. *Curr. Opin. Cell Biol.* 20:35–40.
25. Meinhardt, H. 1999. Orientation of chemotactic cells and growth cones: models and mechanisms. *J. Cell Sci.* 112:2867–2874.
26. Beta, C., G. Amselem, and E. Bodenschatz. 2008. A bistable mechanism for directional sensing. *New J. Phys.* 10:083015.
27. Gamba, A., A. de Candia, …, G. Serini. 2005. Diffusion-limited phase separation in eukaryotic chemotaxis. *Proc. Natl. Acad. Sci. USA.* 102:16927–16932.

28. Xiong, Y., C.-H. Huang, …, P. N. Devreotes. 2010. Cells navigate with a local-excitation, global-inhibition-biased excitable network. *Proc. Natl. Acad. Sci. USA.* 107:17079–17086.

29. Hecht, I., D. A. Kessler, and H. Levine. 2010. Transient localized patterns in noise-driven reaction-diffusion systems. *Phys. Rev. Lett.* 104:158301.

30. Matsuoka, S., T. Shibata, and M. Ueda. 2009. Statistical analysis of lateral diffusion and multistate kinetics in single-molecule imaging. *Biophys. J.* 97:1115–1124.

31. Vazquez, F., S. Matsuoka, …, P. N. Devreotes. 2006. Tumor suppressor PTEN acts through dynamic interaction with the plasma membrane. *Proc. Natl. Acad. Sci. USA.* 103:3633–3638.

32. Shoval, O., L. Goentoro, …, U. Alon. 2010. Fold-change detection and scalar symmetry of sensory input fields. *Proc. Natl. Acad. Sci. USA.* 107:15995–16000.

33. Gillespie, D. T. 2001. Approximate accelerated stochastic simulation of chemically reacting systems. *J. Chem. Phys.* 115:1716–1733.

34. Janetopoulos, C., L. Ma, …, P. A. Iglesias. 2004. Chemoattractant-induced phosphatidylinositol 3,4,5-trisphosphate accumulation is spatially amplified and adapts, independent of the actin cytoskeleton. *Proc. Natl. Acad. Sci. USA.* 101:8951–8956.

35. Fisher, P. R., R. Merkl, and G. Gerisch. 1989. Quantitative analysis of cell motility and chemotaxis in Dictyostelium discoideum by using an image processing system and a novel chemotaxis chamber providing stationary chemical gradients. *J. Cell Biol.* 108:973–984.

36. Parent, C. A., B. J. Blacklock, …, P. N. Devreotes. 1998. G protein signaling events are activated at the leading edge of chemotactic cells. *Cell.* 95:81–91.

37. Meili, R., C. Ellsworth, …, R. A. Firtel. 1999. Chemoattractant-mediated transient activation and membrane localization of Akt/PKB is required for efficient chemotaxis to cAMP in Dictyostelium. *EMBO J.* 18:2092–2105.

38. Takeda, K., D. Shao, …, R. A. Firtel. 2012. Incoherent feedforward control governs adaptation of activated ras in a eukaryotic chemotaxis pathway. *Sci. Signal.* 5:ra2.

39. Parent, C. A., and P. N. Devreotes. 1999. A cell's sense of direction. *Science.* 284:765–770.

40. Levchenko, A., and P. A. Iglesias. 2002. Models of eukaryotic gradient sensing: application to chemotaxis of amoebae and neutrophils. *Biophys. J.* 82:50–63.

41. Hoeller, O., and R. R. Kay. 2007. Chemotaxis in the absence of PIP3 gradients. *Curr. Biol.* 17:813–817.

42. Iijima, M., and P. N. Devreotes. 2002. Tumor suppressor PTEN mediates sensing of chemoattractant gradients. *Cell.* 109:599–610.

43. Tomchik, K. J., and P. N. Devreotes. 1981. Adenosine 3′,5′-monophosphate waves in Dictyostelium discoideum: a demonstration by isotope dilution—fluorography. *Science.* 212:443–446.

44. Goldstein, R. E. 1996. Traveling-wave chemotaxis. *Phys. Rev. Lett.* 77:775–778.

45. Weijer, C. J. 2009. Collective cell migration in development. *J. Cell Sci.* 122:3215–3223.

46. Segall, J. E., S. M. Block, and H. C. Berg. 1986. Temporal comparisons in bacterial chemotaxis. *Proc. Natl. Acad. Sci. USA.* 83:8987–8991.

47. Oono, Y. 2012. The Nonlinear World. Springer, New York.

48. Swanson, J. A., and D. L. Taylor. 1982. Local and spatially coordinated movements in Dictyostelium discoideum amoebae during chemotaxis. *Cell.* 28:225–232.